

# Resolution limits in astronomical images

A.P. Lobanov

Max-Planck-Institut für Radioastronomie, Auf dem Hügel 69, Bonn 53121, Germany

Received  $\langle$ date $\rangle$  / Accepted  $\langle$ date $\rangle$

**Abstract.** A method is introduced to derive resolution criteria for various *a priori* defined templates of brightness distribution fitted to represent structures and objects in astronomical images. The method is used for deriving criteria for the minimum and maximum resolvable sizes of a template. The minimum resolvable size of a template is determined by the ratio of  $(SNR - 1)/SNR$ , and the maximum detectable size is determined by the ratio of  $1/SNR$ . Application of these criteria is discussed in connection to data from filled-aperture instruments and interferometers, accounting for different aperture shapes and the effects of Fourier sampling, tapering, apodization and visibility weighting. Specific resolution limits are derived for four different templates of brightness distribution: (1) two-dimensional Gaussian, (2) optically thin spherical shell, (3) disk of uniform brightness, and (4) ring. The limiting resolution for these templates changes with SNR similarly to the quantum limit on resolution. Practical application of the resolution limits is discussed in two examples dealing with measurements of maximum brightness temperature in compact relativistic jets and assessments of morphology of young supernova remnants.

**Key words.** methods: data analysis – methods: analytical – techniques: high angular resolution – techniques: interferometric

## 1. Introduction

Accurate knowledge of resolution limits is one of the important aspects of astronomical observations and data analysis. There is a number of research fields in which a quantitative assessment of resolution limits is vital for interpretation of observations. Most celebrated examples include the star/galaxy separation in imaging surveys (e.g. Stoughton et al. 2002), measurements of stellar diameters (e.g. Tango & Davis 2002), measurements of sizes and shapes of young supernova remnants (e.g. Marcaide et al. 1995, McDonald et al. 2001, Pérez-Torres et al. 2002, Bartel & Bietenholz 2003), and estimates of brightness temperatures in extragalactic jets based on very long baseline interferometry (VLBI) measurements of sizes of most compact regions (cores) of the jets (e.g. Moellenbrock et al. 1996, Lobanov et al. 2000, Horiuchi et al. 2004)

The Rayleigh (1879) resolution criterion and its several modifications are commonly considered as a measure of limiting resolution. The Rayleigh limit is expressed by the resolution distance  $R = 1.22(\lambda/2\alpha_f)$ , where  $\lambda$  is the wavelength of light and  $\alpha_f = D/f$  is the ratio of the diffracting aperture,  $D$ , to the distance,  $f$ , between the aperture and the image plane. Strict application of the Rayleigh criterion is limited to the specific case of resolving two point-like objects of comparable brightness. In terms of Fourier optics, resolution is better represented by the *instrumental bandwidth* that represents the range of Fourier frequencies sampled by an imaging apparatus. Diffraction results in existence of the maximum

(cutoff) frequency  $q_{\max}$  that limits the resolution. Indeed, the Rayleigh limit has been reformulated, in Fourier optics, in terms of the *Nyquist distance*  $R = \pi/q_{\max}$ . Linear inversion methods applied to *out-of-band extrapolation* yield resolution limits smaller than the one prescribed by  $R$ . This provides the basis of the so-called “superresolution” techniques (Bertero & De Mol 1996 and references therein).

In many practical cases, an observed brightness distribution has to be tested against a specific, extended pattern, for instance, a characteristic surface brightness distribution of a galaxy, stellar disk or supernova shell. A number of astronomical studies employ fitting image brightness distribution by such pre-defined templates, with the definitions being based on physical models or previous observational evidence. Introducing *a priori* knowledge (or a postulate) of the brightness distribution of an emitting region is similar to using the out-of-band extrapolation (in which a definitive postulate is employed about the shape of the emitting region). In both cases, the limiting resolution depends on the signal-to-noise (SNR) of detection. In contrast to the out-of-band extrapolation, the limiting resolution for *a priori* defined templates is determined ultimately by quantum fluctuations of light (Kolobov & Fabre 2000), because the templates are represented by analytic functions that can be extended over an infinite range of frequencies in Fourier domain.

An analytical criterion for calculating resolution limits can be derived for specific templates of brightness distribution (TBD, hereafter) from their respective Fourier visibility representations (see e.g. Thompson, Moran, Swensson 1986, Taylor, Carilli, Perley 1999). Working in the Fourier plane has a spe-

cific advantage of separating positional information (contained in the visibility phase) from information about the extent of the emitting region (contained in visibility amplitudes). This has been recognized early on in radio interferometry and used for a variety of purposes, most notably for error estimates (see e.g. Fomalont 1999).

Analysis of visibility distribution in Fourier domain is applied in this paper to derive general resolution criteria and obtaining resolution limits for specific TBD. The basic foundations of the method for deriving the resolution limits are summarized in Sect. 2. The general resolution criteria are introduced in Sect. 3 for determining the minimum and maximum resolvable size of a TBD. Several relevant TBD are described in Sect. 4. Their respective limiting resolutions are calculated in Sect. 5 and compared with the quantum limits on resolution. Applications of the resolution limits are outlined, in Sect. 6, with two examples dealing with studies of brightness temperature in compact AGN and assessment of morphology of young supernovae.

## 2. Basic definitions

Consider an emitting region of finite size that has an integral flux density  $F$  and a brightness distribution  $I(l, m)$ . The brightness distribution  $I(l, m)$  is measured in the image plane, which is described by a rectangular coordinate system  $(l, m)$ . The corresponding Fourier (or interferometric) visibility distribution  $V(u, v)$  is measured in Fourier plane ( $uv$ -plane), with the respective rectangular coordinate system  $(u, v)$ . The two are related via Fourier transform ( $\mathcal{F}$ ):

$$V(u, v) = \mathcal{F} I(l, m) = \int_{-\infty}^{\infty} \int_{-\infty}^{\infty} I(l, m) \exp[-2\pi i(u l + v m)] dx dy,$$

$$I(l, m) = \mathcal{F}^{-1} V(u, v) = \int_{-\infty}^{\infty} \int_{-\infty}^{\infty} V(u, v) \exp[2\pi i(u l + v m)] dx dy.$$

The visibility distribution is complex-valued, with the visibility amplitude determining the limiting resolution and the visibility phase affecting ultimately the positional accuracy in the image plane. For a circularly symmetric brightness distribution, the relation between  $V(u, v)$  and  $I(l, m)$  can be represented by Hankel transforms

$$V(q) = \int_0^{\infty} I(r) J_0(2\pi q r) r dr,$$

$$I(r) = \int_0^{\infty} V(q) J_0(-2\pi q r) q dq,$$

where  $J_0$  is the zero order Bessel function and  $q = (u^2 + v^2)^{1/2}$  and  $r = (x^2 + y^2)^{1/2}$  are radial coordinates in the Fourier plane and image plane, respectively. For simplicity of derivation, circular symmetry will be assumed throughout this paper, but the method of analysis is valid for the general case as well, which can be readily shown by expanding the variables  $r$  and  $q$  into their two dimensional representations  $(l, m)$  and  $(u, v)$ .

The relevant range  $(q_{\min}, q_{\max})$  of frequencies (coordinate dimensions) in the visibility plane is specific to each individual observational setup. In most of the practical cases,  $q_{\min} \rightarrow 0$  or  $q_{\min} \ll q_{\max}$  can be assumed. For filled-aperture instruments,

$q_{\max}$  is determined by the ratio  $D/\lambda_{\text{obs}}$  of the diameter of the aperture to the observing wavelength. For interferometers, the diameter is substituted by the maximum baseline length,  $B_{\max}$ , between individual elements. If  $q_{\max}$  is known, the Fourier transform of the brightness distribution in an astronomical image can be used for deriving rigorous resolution criteria for a TBD. To convert the result to angular units in the image plane,  $q_{\max}$  has to be related to the size of the point spread function (PSF) or the synthesised beam, in the terminology adopted in radio interferometry. This can be achieved by considering the interferometric visibility sampling function (SF) — an effective coverage of the Fourier plane, which is often also termed as the transfer function. The theoretical shape of the PSF is completely determined by the combination of the SF and the frequency range  $(q_{\min}, q_{\max})$ . In practice, the shape and size of the PSF are further modified by aberrations, weighting and tapering (apodization) of data (e.g. Norton & Beer 1976, Briggs 1995, Briggs, Schwab & Sramek 1999), which also affects actual resolution limits. These effects have to be taken into account, thus reformulating  $q_{\max}$  in terms of the PSF.

### 2.1. Sampling of the Fourier domain

The shape of the PSF,  $B(l, m)$ , depends on the SF (or  $uv$ -distribution)  $s(u, v)$  in the Fourier domain. The PSF is then, in the simplest case,  $B(l, m) = \mathcal{F} s(u, v)$ . The PSF is characterized by its width at half power level (FWHM), which is often also termed the “half power beam width”(HPBW, hereafter). Generally, the two-dimensional shape of the PSF must be considered, and resulting directional resolution limits should be derived. If this is not feasible, an equivalent circular HPBW,  $\mathcal{B}_c$ , can be used, which depends on the actual shape of the PSF or, more generally, on the shape of the SF.  $\mathcal{B}_c$  gives then a corresponding size of a circular PSF that contains the same integrated flux density as the elliptical (or generally speaking, non-circular PSF and SF). For an elliptical SF,

$$\mathcal{B}_c = (a b)^{1/2}, \quad (1)$$

where  $a$  and  $b$  are the major and minor axes of the PSF. For a rectangular SF,

$$\mathcal{B}_c = (\pi a b)^{1/2}. \quad (2)$$

Equations (1) and (2) can be applied to describe  $\mathcal{B}_c$  of most of the imaging instruments used in astronomy.

The relation between the beam and the sampling function is even more complex if  $s(u, v)$  provides either incomplete or non-uniform coverage of the Fourier plane. The visibility sampling can then be characterized by the smallest and largest  $uv$ -distances ( $q_{\min}, q_{\max}$ ) and by the density  $\rho_{\sigma}(u, v)$  of the  $uv$ -samples (assuming  $q_{\max} \gg q_{\min}$ ). The density is defined so that  $\rho_{\sigma}(u, v) du dv$  gives the number of visibilities within the area given by  $(u \pm 0.5du, v \pm 0.5dv)$ . The visibility sampling can be modified by a weighting function  $w(u, v)$  to emphasize certain fractions of the visibility distribution and optimize image sensitivity on selected spatial scales. With the weighting function applied,

$$s(u, v) = \rho_{\sigma}(u, v)w(u, v), \quad (3)$$

giving the total number of visibility data points  $N(u, v) = \int \int s(u, v) du dv$ .

Depending on the form of  $s(u, v)$ , an appropriate correction factor  $\mathcal{S}_q$  must be applied to the equivalent (or directional) HPBW  $\mathcal{B}_c$ , which gives

$$q_{\max} = (\mathcal{S}_q \mathcal{B}_c)^{-1}. \quad (4)$$

## 2.2. $\mathcal{S}_q$ for a power law $s(u, v)$

A power-law SF can be used to describe an ideal interferometer as well as a major fraction of single aperture instruments. The effect of a power-law SF on the HPBW can be calculated analytically. Assuming circular symmetry yields  $s(q) = \rho_\sigma(q) w(q)$ . The density of samples is  $\rho_\sigma(q) \propto q^{-2}$ . The function  $w(q)$  is then given by  $q^\beta$ , where  $\beta$  is a power index describing the weighting. The choice of  $w(q)$  that yields  $s(q) = \text{const}$  is commonly known as “natural weighting”. Thus,  $\beta = 2$ , for the natural weighting, and the corresponding  $s(q)$  is given by  $\Pi(q)$ , where  $\Pi(q) = H(1+q)H(1-q)$  and  $H$  is the unit Heaviside function. The natural weighting increases sensitivity to extended emission at the expense of reducing the resolution of the image. The resolution is optimized by choosing  $w(q) = \text{const}$  (uniform weighting), for which the respective  $s(q) = \rho_\sigma(q)$ . This yields  $s(q) \propto q^{-2}$  for the uniformly weighted synthesised interferometric aperture (similar to the result obtained for filled aperture telescopes). A general form of the sampling function is then

$$s(q) = \Pi(q) w(q) \rho_\sigma q dq = \Pi(q) q^{\beta-2} dq, \quad (5)$$

with  $\beta = 0$  for the uniform weighting and  $\beta = 2$  for the natural weighting. Thus, for a power law  $s(q)$  given by Eq. (5),

$$\mathcal{S}_q = 2^{1-\beta/2}, \quad (6)$$

and  $q_{\max}$  is related to the effective HPBW as follows:

$$q_{\max} = \frac{1}{2^{1-\beta/2} \mathcal{B}_c}, \quad (7)$$

where  $a$  and  $b$  are the major and minor axes of the synthesised beam. For filled aperture instruments,  $\beta = 0$  and  $\mathcal{S}_q = 1/2$  can be generally adopted.  $\mathcal{S}_q$  can be modified by apodization, depending on the shape and parameters of the apodizing function. The range of  $\beta$  [0, 2] corresponds to a range [-1, 1] of the *robustness parameter* introduced by Briggs (1995).

In interferometers, the shape of the SF may deviate from the power-law due to several factors including sparsity of receiving elements, non-optimal configurations, and reduced mutual visibility on very long baselines. A relative error  $\sigma_q$  of  $\mathcal{S}_q$  due to an incomplete SF of an interferometer can be approximated from the size of gaps  $\Delta q/q$  in the SF. For an interferometer with  $N$  regularly spaced elements,  $\sigma_q \approx (\Delta q/q)^2 = [(q_{\max}/q_{\min})^{3/N} - 1]^2$  (Lobanov 2003<sup>1</sup>). The resulting  $\sigma_q$  is a few per cent or less for most of the existing connected interferometers. It is expected to be improved substantially in the future interferometric instruments such as ALMA and SKA. In present-day VLBI observations,  $\sigma_q$  remains about 10%–15%.

Thus, Eq. (6) provides a relatively accurate assessment of  $\mathcal{S}_q$ . Numerical analysis of the specific instrumental SF should be employed whenever a better accuracy is required.

## 2.3. Noise and SNR

The Fourier transform has a fundamental property of preserving the covariance of noise. It implies that the signal-to-noise ratio (SNR) measured in the image plane is the same as the one that would have been recovered if the same structure was fitted to the data in the visibility plane. Then  $\text{SNR} = F/\sigma_n = V(0)/\sigma_n$ , which is the ratio of the integral flux density to the variance of the additive white Gaussian noise with a power spectrum  $\rho(q) = \sigma_n^2 \delta(q)$ . This property enables the derivation of resolution criteria from the Fourier transform of the image brightness distribution. It should be noted that the definition of SNR introduced above is different from another commonly used definition given by  $I(0)/\sigma_n$ .

The full SNR is applied for calculation of the resolution limits if the brightness distribution is fit by a single template or if the position of the template of interest is fixed, in a fit by multiple templates. If the brightness distribution is fit by multiple templates at variable positions, the SNR in the estimates of  $d_{\text{lim}}$  and  $d_{\text{res}}$  should be multiplied by a factor  $\eta = \sqrt{1 - \sigma_{\text{phase}}^2/\sigma_{\text{amp}}^2}$ , where  $\sigma_{\text{phase}}$  and  $\sigma_{\text{amp}}$  is the noise in the visibility phases and amplitudes, respectively. Typically, the noise is distributed evenly between the amplitudes and phases, and so  $\sigma_{\text{phase}} = \sigma_{\text{amp}} = \sigma_n/\sqrt{2}$  and  $\eta = 1/\sqrt{2}$ .

## 3. Resolution criteria

Consider a circularly symmetric object in the image plane, which has an integral flux density  $F$  and a distribution of brightness  $I(r)$  that transforms into a visibility distribution  $V(q)$ . The noise is given by  $\sigma_n$ . The visibility distribution  $V(q)$  is normalized by  $F$ , implying  $V(0) \equiv 1$ . The visibility distribution can be conveniently represented as

$$V(q) = d \mathcal{V}_s(q), \quad (8)$$

where  $\mathcal{V}_s$  and  $d$  represent the shape and size of a TBD, respectively.

### 3.1. Minimum resolvable size

For a point-like brightness distribution,  $I(r) = \delta(r)$ ,  $V(q) \equiv 1$  at all  $q$ . For an object with extended brightness distribution,  $V(q) = 1 - \xi(q)$ , where  $\xi(q)$  depends on the size and shape of the object. If this deviation of the visibility distribution from unity can be detected in the data, then the brightness distribution  $I(r)$  is resolved. The function  $\xi(q)$  evaluated at  $q_{\max}$  can be related to the SNR of detection of the TBD. The resolution criterion is then given by  $\xi(q_{\max}) \geq \sigma_n = 1/\text{SNR}$ . This criterion implies that  $I(r)$  is resolved if

$$V(q_{\max}) \leq \frac{\text{SNR} - 1}{\text{SNR}} \equiv f_m(\text{SNR}). \quad (9)$$

Solving this equation for  $d$ , recovered from the expression for  $V(q_{\max})$ , yields the limiting resolution  $d_{\text{lim}}$  for a given template.

<sup>1</sup> [http://www.skatelescope.org/PDF/ska\\_memo38.pdf](http://www.skatelescope.org/PDF/ska_memo38.pdf)

Following Eq. (8),  $V(q_{\max}) = d_{\lim} q_{\max} \mathcal{V}_s$ , and the limiting resolution is

$$d_{\lim} = \frac{1}{q_{\max}} \frac{f_m(SNR)}{\mathcal{V}_s}. \quad (10)$$

The form  $\mathcal{V}_s$  depends on the choice of the template. The ratio

$$\mathcal{R}_{\lim} = \frac{f_m(SNR)}{\mathcal{V}_s} \quad (11)$$

provides a theoretical resolution factor independent from the size and shape of the PSF of the data.  $\mathcal{R}_{\lim}$  depends only on the SNR and the shape of a TBD.  $\mathcal{R}_{\lim}$  is a measure of the space-bandwidth product  $c = d q_{\max}$ . Indeed  $\mathcal{R}_{\lim} = 2 c_{\lim}$ . This elucidates the connection between  $\mathcal{R}_{\lim}$  and the Shannon number,  $S = d/R$ , which gives, for a spatial interval  $[-d/2, +d/2]$ , the number of sampling points that are separated by the Nyquist distance  $R = \pi/q_{\max}$  (Toraldo di Francia 1969). It follows immediately that

$$\mathcal{R}_{\lim} = \pi S_{\lim}, \quad (12)$$

where the subscript in  $S$  implies that the Shannon number is evaluated at  $d_{\lim}$ . Recalling Eq. (4), the resolution limit can be rewritten as

$$d_{\lim} = \mathcal{R}_{\lim} S_q \mathcal{B}_c. \quad (13)$$

The HPBW given by  $\mathcal{B}_c$  can represent both the FWHM of a non-circular PSF along a selected direction in the image plane or an equivalent of the FWHM of a circular PSF calculated using Eqs. (1–2). The term  $S_q$  accounts for the effect of limited sampling of the Fourier domain (see Sect. 2.2).

### 3.2. Largest detectable size

Visibility amplitude of a completely resolved template reaches  $\sigma_n$  at a scale  $q_{\text{res}}$  such that  $q_{\text{res}} \leq q_{\max}$ . This yields a resolution condition

$$V(q_{\text{res}}) = \sigma_n = \frac{1}{SNR} \equiv f_r(SNR). \quad (14)$$

The largest detectable size is obtained by using Eq. (8) to separate different terms in  $V(q_{\text{res}})$ , which gives

$$d_{\text{res}} = \frac{1}{q_{\text{res}}} \frac{f_r(SNR)}{\mathcal{V}_s}, \quad (15)$$

similar to Eq. (10). The main difference from Eq. (10) is that  $f_r(SNR)/\mathcal{V}_s$  cannot now be used as an SNR-dependent resolution factor separately from  $q_{\text{res}}$ , since the latter also depends on the SNR of the detection. Evidently,  $SNR = \sqrt{N(q_{\max})/N(q_{\text{res}})}$  is required for a fully resolved template to be detected at  $q_{\text{res}}$ . Here,  $N(q_{\max})$  and  $N(q_{\text{res}})$  are the numbers of visibility samples within  $q_{\max}$  and  $q_{\text{res}}$ , respectively. The value of  $q_{\text{res}}$  depends on the sampling function  $s(q)$ , and it can be found by solving the equation  $N(q) = \int_0^q s(q) dq$  for the upper limit of integration.

Alternatively,  $q_{\text{res}}$  can be expressed as a combination of SNR and  $q_{\max}$ , with the latter being conveniently related to the HPBW using Eq. (4). For instance, for a power-law  $s(q)$  given by Eq. (5),

$$q_{\text{res}} = \frac{q_{\max}}{SNR^{1/(3-\beta)}}, \quad (16)$$

and the largest resolvable size is then given by

$$d_{\text{res}} = \frac{SNR^{1/(3-\beta)} f_r(SNR)}{\mathcal{V}_s} S_q \mathcal{B}_c. \quad (17)$$

An equivalent of the SNR-dependent resolution factor  $\mathcal{R}$  can now be defined by

$$\mathcal{R}_{\text{res}} = \frac{SNR^{1/(3-\beta)} f_r(SNR)}{\mathcal{V}_s}, \quad (18)$$

transforming Eq. (17) into the same form as Eq. (13). By analogy with Eq. (12),

$$\mathcal{R}_{\text{res}} = \pi S_{\text{res}}. \quad (19)$$

The limit  $d_{\text{res}}$  signifies the largest size of a template that can be detected. At sizes larger than  $d_{\text{res}}$ , sensitivity to extended emission becomes insufficient to detect the specific shape of brightness distribution described by the template. In case of fitting astronomical data by multiple templates (e.g. in “modelfitting” used in radio interferometry; see Pearson 1999),  $d_{\text{res}}$  gives an estimate of the size at which a template must be split into two templates, to maintain an adequate representation of the structure observed. The ratio  $d_{\text{res}}/d_{\lim}$  defines an effective “resolution dynamic range” (RDR),  $\mathcal{D}$ , that expresses the range of template sizes that can be detected at a given SNR. The RDR depends only on the SNR of detection and the data weighting, since the terms related to HPBW, SF, and the shape of the template ( $\mathcal{V}_s$ ) all cancel in the ratio, giving

$$\mathcal{D} = \frac{\mathcal{R}_{\text{res}}}{\mathcal{R}_{\lim}}. \quad (20)$$

## 4. Relevant templates of brightness distribution

There are several commonly used TBD for describing structures observed in astronomical images (particularly in VLBI images). These include a two-dimensional Gaussian profile (“Gaussian component”), a disk of uniform brightness, an optically thin sphere (or shell of finite thickness), and a ring (see Pearson 1999). Gaussian components are commonly used to approximate and quantify structures recovered in VLBI images of relativistic jets and other objects. Shells, disks and rings are applied to analysis of images of supernovae and stellar objects.

### 4.1. Gaussian component

A circular Gaussian shape with the FWHM  $d$  is given by

$$I(r) = \frac{2 \sqrt{\ln 2}}{\sqrt{\pi} d} \exp\left(\frac{-4 \ln 2 r^2}{d^2}\right) = \frac{C_{\sigma}}{d} \exp\left(\frac{-\pi C_{\sigma}^2 r^2}{d^2}\right), \quad (21)$$

with  $C_{\sigma} = 2 \sqrt{\ln(2)/\pi}$ . An elliptical Gaussian component  $I(r, \phi)$  can be described substituting  $d$  with the running FWHM

$$d_{\phi} = \sqrt{[a \cos(\phi - \psi)]^2 + [b \sin(\phi - \psi)]^2}, \quad (22)$$

where  $a, b$  are the major and minor axes of the component and  $\psi$  is the position angle of the major axis. The visibility distribution corresponding to the Gaussian component is

$$V(q) = \exp\left(\frac{-(\pi d_{\phi} q)^2}{4 \ln 2}\right) = \exp\left(-\frac{\pi d_{\phi}^2 q^2}{C_{\sigma}^2}\right). \quad (23)$$

An equivalent of circular FWHM can be obtained in this case by finding the corresponding diameter of a circular Gaussian which has the same area at the half-power level. This gives  $d_{\text{FWHM}} = \sqrt{ab}$ .

#### 4.2. Spherical shell of finite thickness

A homogeneous shell with the outer radius  $r_s$  and a thickness  $\delta_r r_s = (1 - \alpha)r_s$  (with  $0 \leq \alpha \leq 1$ ) is described by

$$I(r) = \begin{cases} f_{r_s}(r) - f_{\alpha r_s}(r) & r \leq r_s, \\ 0 & r > r_s \end{cases} \quad (24)$$

with  $f_z(r) = \sqrt{z^2 - r^2}$ . Thus,  $\alpha = 0$  describes an infinitely thin shell and  $\alpha \rightarrow 1$  describes a filled sphere. The respective visibility distribution is given by Hankel transform of Eq. (24), which yields

$$V(q) = \xi_V \frac{1}{8\pi^3 q^3} [\sin(2\pi r_s q) - 2\pi r_s q \cos(2\pi r_s q) - \sin(2\pi \alpha r_s q) + 2\pi \alpha r_s q \cos(2\pi \alpha r_s q)], \quad (25)$$

where  $\xi_V = 3/[r_s^3(1 - \alpha^3)]$  is the normalization factor derived from the condition  $V(0) = 1$ . If the shell is described by its outer diameter  $d = 2r_s$ , then  $f_z = \sqrt{z^2 - d^2/4}$ , and

$$V(q) = \frac{3}{(1 - \alpha^3)\pi^3 d^3 q^3} [\sin(\pi d q) - \pi d q \cos(\pi d q) - \sin(\alpha \pi d q) + \alpha \pi d q \cos(\alpha \pi d q)], \quad (26)$$

For small  $d$  ( $d \leq \text{HPBW}$ ),  $V(q)$  can be approximated by the Taylor expansion

$$V(q) = 1 - \frac{1}{10} \left( \frac{1 - \alpha^5}{1 - \alpha^3} \right) \pi^2 d^2 q^2 + o(q^4). \quad (27)$$

#### 4.3. Disk of uniform brightness

A uniformly bright disk of diameter  $d$  is described by

$$I(r) = \begin{cases} 4/(\pi d^2), & r \leq d, \\ 0 & r > d. \end{cases} \quad (28)$$

The corresponding visibility distribution is

$$V(q) = \frac{2 J_1(\pi d q)}{\pi d q}, \quad (29)$$

where  $J_1$  is the Bessel function of the first kind. A useful approximation of  $V(q)$  in the small-size limit is given by the Taylor expansion

$$V(q) = 1 - \frac{(\pi d q)^2}{8} + o(q^4). \quad (30)$$

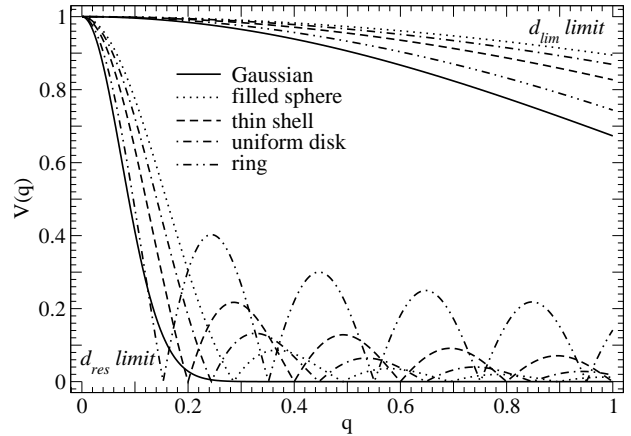


**Fig. 1.** Visibility amplitudes  $V(q)$  of the templates plotted for the small-size ( $d_{\text{lim}}$ ) and large-size ( $d_{\text{res}}$ ) limits.

#### 4.4. Ring

In a ring of diameter  $d$ , the brightness is zero everywhere except on the circumference:

$$I(r) = \frac{1}{\pi d} \delta(r - d/2). \quad (31)$$

The respective visibility distribution is given by

$$V(q) = J_0(\pi d q), \quad (32)$$

and it can be approximated conveniently using the Taylor expansion of the Bessel function

$$J_0(\pi d q) = 1 - \frac{(\pi d q)^2}{4} + o(q^4). \quad (33)$$

The visibility amplitudes of all five templates are compared in Fig. 1, which illustrates the behavior of  $V(q)$  in the small-size and large-size limits (corresponding to the conditions used for deriving  $d_{\text{lim}}$  and  $d_{\text{res}}$ , respectively. It should be noted that the third order Taylor expansions used above approximate well the shape of  $V(q)$  only in the small-size limit. Thus, only  $d_{\text{lim}}$  derived from the Taylor approximations of  $V(q)$  are accurate. In the large-size limit, analytical expressions obtained with  $V(q)$  given by Eqs. (27), (30) and (33) underestimate  $d_{\text{res}}$  by up to 40%. To remove this inaccuracy, numerical solutions must be obtained for  $d_{\text{res}}$  of the shell, disk and ring templates. The numerical solutions can then be used to derive empirical correction functions for the analytical expressions for  $d_{\text{res}}$ . These correction functions are derived in Appendix A. The corrected  $d_{\text{res}}$  are accurate to within 0.01%.

#### 4.5. Noise term in Taylor expansions of $V(q)$

The  $o(q^4)$  term in the Taylor expansions used for approximating  $V(q)$  must be expressed in terms of  $\sigma_n$  or SNR, in order to be included into the derivation of  $d_{\text{lim}}$ . The  $o(q^4)$  term reflects the error of the Taylor approximation of  $V(q)$ . Since  $q$  represents a position in the two-dimensional Fourier plane, the error is proportional to the area  $\sigma_n^2$  of the region described by  $o(q^4)$ ,

modified by the uncertainty  $1/(1 - \sigma_n)$  in the border of that region. Therefore,  $o(q^4)$  can be expressed as follows:

$$o(q^4) = \frac{\sigma_n^2}{1 - \sigma_n} = \frac{1}{SNR(SNR - 1)}. \quad (34)$$

As was discussed above, application of the Taylor expansions is restricted to the small-size limit, and the representation of  $o(q^4)$  given by Eq. (34) can only be used for estimating  $d_{\text{lim}}$ . Estimates of  $d_{\text{res}}$  derived with this representation would diverge at small SNR.

## 5. Resolution limits

The resolution criteria given by Eqs. (9) and (14) can be applied to derive specific resolution limits for the templates described above. Analytical solutions can be found for these equations, following the method outlined in Sect. 3.1–3.2. If analytical expressions for  $d_{\text{lim}}$  and  $d_{\text{res}}$  are computationally inconvenient or cannot be found, the limits can be obtained numerically. Numerical solutions should then be obtained for an effective HPBW = 1, thus requiring

$$q_{\text{max}} = \frac{1}{\sqrt{\pi}} \frac{1}{2^{1-\beta/2}} \quad (35)$$

to be set for estimating  $d_{\text{lim}}$ . For  $d_{\text{res}}$

$$q_{\text{res}} = \frac{1}{\sqrt{\pi}} \frac{1}{2^{1-\beta/2}} \frac{1}{S^{1/(3-\beta)}} \quad (36)$$

should be set. Equations (9) and (14) can be then solved numerically for  $d_{\text{lim}}$  and  $d_{\text{res}}$  expressed in units of HPBW. The corresponding resolution factors are obtained from

$$\mathcal{R}_{\text{lim}} = d_{\text{lim}} \frac{\sqrt{\pi}}{2^{2-\beta/2}}, \quad \mathcal{R}_{\text{res}} = d_{\text{res}} \frac{\sqrt{\pi}}{2^{2-\beta/2}}. \quad (37)$$

These numerical solutions can be calculated for a relevant range of SNR, and the dependences of  $d_{\text{lim}}$  and  $d_{\text{res}}$  on SNR can be established.

This section and Appendix A summarize the analytical resolution limits obtained for the templates described in Sect. 4. For each template, general forms of  $d_{\text{lim}}$  and  $d_{\text{res}}$  and their respective  $\mathcal{R}_{\text{lim}}$  and  $\mathcal{R}_{\text{res}}$  are listed. In all specific examples, a rectangular, power-law SF given by Eq. (5) is adopted, with  $\mathcal{B}_c$  given by Eq. (2) and the SF correction factor  $\mathcal{S}_q$  described by Eq. (6). The uniform weighting ( $\beta = 0$ ) is assumed in all examples. This corresponds, with a high degree of accuracy, to astronomical images with a Gaussian PSF.

### 5.1. Gaussian component

$$d_{\text{lim}} = \frac{2}{\pi} \left[ \ln 2 \ln \left( \frac{SNR}{SNR - 1} \right) \right]^{1/2} \mathcal{S}_q \mathcal{B}_c, \quad (38)$$

$$\mathcal{R}_{\text{lim}} = \frac{2}{\pi} \left[ \ln 2 \ln \left( \frac{SNR}{SNR - 1} \right) \right]^{1/2}. \quad (39)$$

For a rectangular, power-law SF, this corresponds to

$$d_{\text{lim}} = \frac{2^{2-\beta/2}}{\pi} \left[ \pi a b \ln 2 \ln \left( \frac{SNR}{SNR - 1} \right) \right]^{1/2}. \quad (40)$$

For the uniform weighting, Eq. (40) yields a “benchmark” value of  $d_{\text{lim}} = 1$  HPBW at SNR = 4.

#### 5.1.1. Resolution limit in the image domain

For the specific case of a Gaussian template fitted to an image with a Gaussian PSF,  $d_{\text{lim}}$  can be derived in the image plane as well. Consider the maximum difference between the Gaussian PSF,  $I_b(r)$ , and a Gaussian template,  $I_f(r)$ , convolved with the PSF. In this case, the deconvolved size,  $d_f$ , of the template can be conveniently expressed in units of FWHM of the PSF, thus setting the HPBW  $d_b = 1$ . This corresponds to a Gaussian with a FWHM  $d_i = \sqrt{1 + d_f^2}$  fitted directly to the image. Normalizing the peak flux density and the PSF to  $I_f(0) = I_b(0) = 1$  gives  $SNR = 1/\sigma_n$ . This normalization can be used for all  $d_f$  smaller than, or comparable with, the HPBW. The PSF is then described by

$$I_b(r) = C_\sigma \exp \left( -4 \ln 2 \frac{r^2}{1} \right) \quad (41)$$

and the template is given by

$$I_f(r) = C_\sigma \exp \left( -4 \ln 2 \frac{r^2}{1 + d_f^2} \right). \quad (42)$$

The template will be resolved in the image if  $I_f - I_b \geq \sigma_n$  at least at one point. The maximum difference between  $I_f$  and  $I_b$  is realised at  $r = 1/\sqrt{2}$ , and so the resolution condition becomes

$$I_f - I_b = \left( \frac{1}{4} \right)^{1/(1+d_f^2)} - \left( \frac{1}{4} \right) = \frac{\sigma_n}{C_\sigma} = \frac{1}{C_\sigma SNR}. \quad (43)$$

Solving for  $d_{\text{lim}} = d_f$  gives the

$$d_{\text{lim}} = \left[ \frac{\ln(1/4)}{\ln(\sigma_n/C_\sigma + 1/4)} - 1 \right]^{1/2} = \left[ \frac{\ln(4)}{\ln(\frac{4C_\sigma SNR}{4+C_\sigma SNR})} - 1 \right]^{1/2}, \quad (44)$$

measured in units of HPBW. This is the deconvolved size of a Gaussian template, and it can be compared with results from Eqs. (38–40). For SNR = 4, Eq. (44) yields  $d_{\text{lim}} = 1$  HPBW, similarly to Eq. (40) applied to uniformly weighted interferometric data. The two limiting resolutions are essentially identical at  $SNR > 4$  (Fig 2). For  $SNR < 3$ , the asymptotes of Eqs. (38) and (44) are different, and Eq. (44) diverges at  $SNR = 4/3$ . This should be expected, remembering that the normalization used for  $I_b$  and  $I_f$  can only be used for  $d_f$  (and, consequently,  $d_{\text{lim}}$ ) smaller than the HPBW (which necessarily implies  $SNR \geq 4$ ).

For  $d_{\text{lim}}$  given by Eq. (44), the corresponding limiting size of a Gaussian template convolved with the PSF is given by

$$d_{\text{lim,conv}} = \left[ \frac{\ln(4)}{\ln(\frac{4SNR}{4+SNR})} \right]^{1/2}, \quad (45)$$

which is always larger than the HPBW.

#### 5.1.2. Maximum resolvable size and the RDR

$$d_{\text{res}} = \frac{2}{\pi} \left[ \ln 2 SNR^{2/(3-\beta)} \ln(SNR) \right]^{1/2} \mathcal{S}_q \mathcal{B}_c, \quad (46)$$

$$\mathcal{R}_{\text{res}} = \frac{2}{\pi} \left[ \ln 2 SNR^{2/(3-\beta)} \ln(SNR) \right]^{1/2}. \quad (47)$$

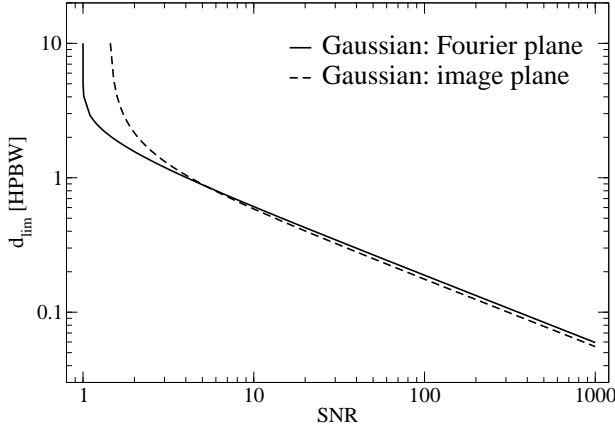


**Fig. 2.** Resolution limits derived for a Gaussian template in the Fourier plane (solid line) and image plane (dashed line). The resolution limit in the Fourier domain is derived for a rectangular SF and the uniform weighting. The resolution limit in the image domain is derived for a Gaussian PSF. At  $\text{SNR} > 4$ , both limits have the same dependence  $d_{\text{lim}} \propto \text{SNR}^{-1/2}$ . At low SNR, the limit derived in the image plane diverges more rapidly because the normalization  $I_b(0) = I_f(0) = 1$  is valid only for  $d_f \lesssim \text{HPBW}$ .

The maximum resolvable size for a rectangular, power-law SF is given by

$$d_{\text{res}} = \frac{2^{2-\beta/2}}{\pi} \left[ \pi a b \ln 2 \text{SNR}^{2/(3-\beta)} \ln(\text{SNR}) \right]^{1/2}. \quad (48)$$

At very high SNR and for poor Fourier domain coverages,  $d_{\text{res}}$  estimated from Eq. (46) can exceed the largest detectable scale  $d_{\text{lds}} = 1/q_{\min}$ . In this case,  $d_{\text{lds}}$  should be used rather than  $d_{\text{max}}$ . The respective RDR obtained from the ratio of  $d_{\text{res}}/d_{\text{lim}}$  given by Eqs. (46) and (40) is then

$$\mathcal{D} = \left[ \text{SNR}^{2/(3-\beta)} \ln(\text{SNR}) / \ln\left(\frac{\text{SNR}}{\text{SNR} - 1}\right) \right]^{1/2}. \quad (49)$$

The RDR is plotted in Fig. 3 for different values of  $\beta$ . For  $\mathcal{D} \leq 1$ , no estimates of size can be made. The SNR levels at which  $\mathcal{D} = 1$  are 1.86, 1.82, and 1.70, for  $\beta = 0, 1, 2$ , respectively. At  $\text{SNR} \geq 10$ , the RDR is  $\propto \text{SNR}^{0.76}$ ,  $\text{SNR}^{0.84}$ , and  $\text{SNR}^{1.09}$  for  $\beta = 0, 1, 2$ , respectively.

## 5.2. Quantum limits on resolution

The dependence of  $d_{\text{lim}}$  on SNR can be compared with the ultimate limit on resolution due to quantum fluctuations of light (Kolobov & Fabre 2000). The effective quantum resolution distance  $R_q = R S / (Q + 1)$ , where  $Q + 1$  is an effective number of degrees of freedom (NDF) in the template (Bertero & De Mol 1996). The Rayleigh limit  $R = \pi/q_{\max} = \pi^{3/2} 2^{1-\beta/2} \sqrt{a b}$ , and this yields the quantum limit of resolution

$$R_q = \pi^{3/2} 2^{1-\beta/2} \frac{S}{Q + 1}, \quad (50)$$

expressed in units of HPBW. The values of  $S$  and  $Q + 1$  are calculated for each SNR and its corresponding  $d_{\text{lim}}$ .  $R_q$  represents then the absolute, quantum limit for resolving an emitting

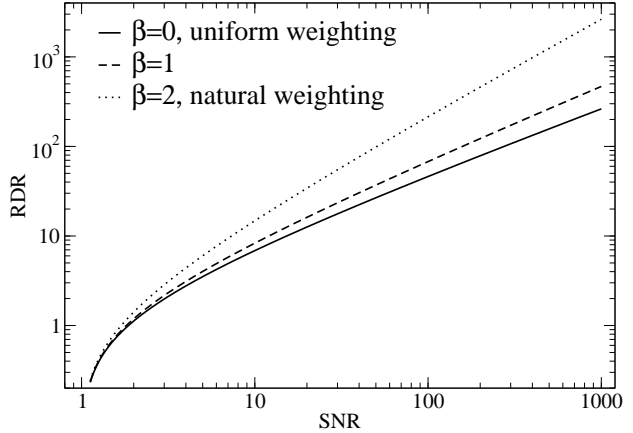


**Fig. 3.** Resolution dynamic range ( $\mathcal{D} = d_{\text{res}}/d_{\text{lim}}$ ) derived for a Gaussian TBD, a rectangular SF and different values of  $\beta$ . At high SNR and for poor Fourier domain coverages,  $d_{\text{res}}$  may exceed  $d_{\text{lds}}$  and should be then substituted by the latter. Valid size estimates are only possible for  $\mathcal{D} \geq 1$ . This corresponds to  $\text{SNR} \geq 1.86, 1.82$ , and  $1.70$ , for  $\beta = 0, 1, 2$ , respectively.

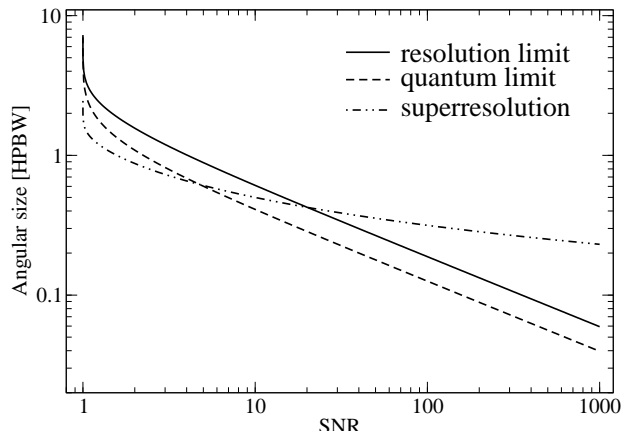


**Fig. 4.** Resolution limit  $d_{\text{lim}}$  for a Gaussian template compared to the quantum limit  $R_q$  of resolution and the superresolution limit for out-of-band extrapolation. At  $\text{SNR} > 3$ , the quantum limit and  $d_{\text{lim}}$  are both  $\propto \text{SNR}^{-1/2}$  and  $d_{\text{lim}} \approx 1.5 R_q$ . The superresolution limit approaching  $\propto \text{SNR}^{-0.1}$  at  $\text{SNR} > 10$ .  $\text{SNR} = 4.76$  marks the lowest limit at which superresolution can be applied, and  $\text{SNR} = 20$  gives the lowest limit for super-resolving a Gaussian brightness profile.

region of finite extent and arbitrary shape detected at a given SNR. The same equation evaluated at  $S = \pi^{3/2} 2^{(\beta-2)/2}$  gives the SNR dependence of the superresolution limit for out-of-band extrapolation. The NDF is evaluated following Kolobov & Fabre (2000) and Frieden (1971) in the quantum limit and following Bertero & De Mol (1996) in the classical limit that applies for superresolution.

The quantum and superresolution limits are compared to  $d_{\text{lim}}$  in Fig. 4. The quantum limit decreases at the same rate as  $d_{\text{lim}}$ , approaching asymptotically to an  $\text{SNR}^{-1/2}$  proportionality at  $\text{SNR} > 3$ . This result agrees well with the theoretical limit on photon number fluctuation in an interferometer given by  $\Delta n \approx n^{-1/2} = \text{SNR}^{-1/2}$  (Forward 1978, Hariharan & Sanders

1996). At  $\text{SNR} > 3$ ,  $d_{\text{lim}} \approx 1.5 R_q$ , thus connecting the resolution criterion for a Gaussian template to the quantum limit. Compared to the quantum limit and  $d_{\text{lim}}$ , the superresolution limit decreases much slower, approaching an  $\text{SNR}^{-0.1}$  dependence at  $\text{SNR} > 10$ . The difference between the two asymptotes results from different strength of assumptions made about the extent and shape of the brightness distribution. The superresolution is not feasible at  $\text{SNR} \leq 4.76$  for an object of arbitrary shape. For a Gaussian (or nearly Gaussian) brightness distribution, application of the superresolution technique is only feasible at  $\text{SNR} \geq 20$ .

### 5.3. Comparison of resolution limits for different templates

Resolution factors and limits for a spherical shell, uniform disk and ring templates described in Sect. 4 are derived in Appendix A. Resolution factors  $\mathcal{R}_{\text{lim}}$  and  $\mathcal{R}_{\text{res}}$  are plotted in Fig. 5 and compared in Tables 1 and 2 for different templates and SNR levels. The Gaussian template has the smallest  $\mathcal{R}_{\text{lim}}$  at all SNR. At  $\text{SNR} \geq 4$ ,  $\mathcal{R}_{\text{lim}} \propto \text{SNR}^{-1/2}$  for all templates. The picture is different for  $\mathcal{R}_{\text{res}}$ . At  $\text{SNR} \rightarrow \infty$ , the asymptotes are  $\mathcal{R}_{\text{res}} \propto \text{SNR}^{0.4}$  for a Gaussian template and  $\mathcal{R}_{\text{res}} \propto \text{SNR}^{0.33}$  for the other templates. This difference is caused by the presence of zeros in the  $V(q)$  of the shell, disk and ring templates (see Fig. 1). The Gaussian template reaches zero at infinity, and thus it can be better detected at large sizes and large SNR, compared to the other three templates.

**Table 1.**  $\mathcal{R}_{\text{lim}}$  for different templates

$\mathcal{R}_{\text{lim}}$	SNR					
	1	3	5	10	$10^2$	$10^3$
Gaussian	$\infty$	0.337	0.250	0.172	0.053	0.016
Sphere	$\infty$	0.712	0.503	0.335	0.101	0.032
Shell	$\infty$	0.551	0.390	0.260	0.078	0.024
Disk	$\infty$	0.637	0.450	0.300	0.090	0.029
Ring	$\infty$	0.450	0.318	0.212	0.064	0.020

**Table 2.**  $\mathcal{R}_{\text{res}}$  for different templates

$\mathcal{R}_{\text{res}}$	SNR					
	1	3	5	10	$10^2$	$10^3$
Gaussian	0	0.801	1.150	1.733	5.279	13.930
Sphere	0	1.396	1.915	2.701	5.540	14.171
Shell	0	1.046	1.413	1.956	4.595	9.913
Disk	0	1.231	1.677	2.345	5.592	12.182
Ring	0	0.831	1.111	1.521	3.524	7.648

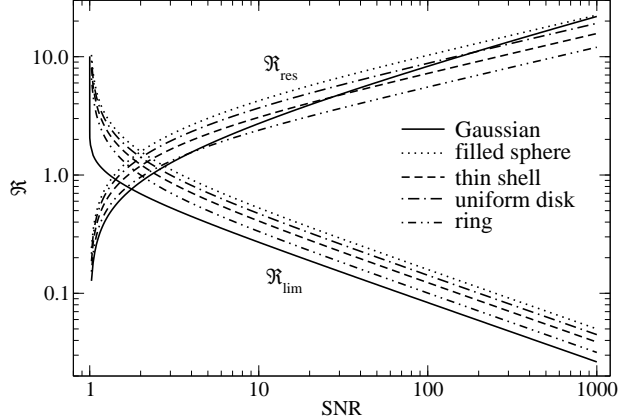


**Fig. 5.** Resolution factors  $\mathcal{R}_{\text{lim}}$  and  $\mathcal{R}_{\text{res}}$  for different templates. At a given SNR, the Gaussian template has the smallest  $\mathcal{R}_{\text{lim}}$ . All templates have similar asymptotics  $\mathcal{R}_{\text{lim}} \propto \text{SNR}^{-1/2}$  at  $\text{SNR} \geq 4$ . For the largest detectable size and  $\text{SNR} \rightarrow \infty$ , the asymptotes are  $\mathcal{R}_{\text{res}} \propto \text{SNR}^{0.4}$  for a Gaussian template and  $\mathcal{R}_{\text{res}} \propto \text{SNR}^{0.33}$  for the other templates. The steeper rise of  $\mathcal{R}_{\text{res}}$  of the Gaussian template compared to the other templates results from the presence of zeros in the  $V(q)$  of the shell, disk, and ring (see Fig. 1).

## 6. Applications

### 6.1. Brightness temperature estimates from VLBI data

Brightness temperature,  $T_b$ , of non-thermal continuum emission is commonly used as an indicator of physical conditions in the emitting material. In relativistic jets, the inverse-Compton limit of  $T_b \approx 10^{12}$  K (Kellermann & Paulini-Toth 1969, Kellermann 2002) is often reached and exceeded, implying angular dimensions smaller than the FWHM of the resolving PSF. In this case, the resolution criteria described by  $\mathcal{R}_{\text{lim}}$  and  $d_{\text{lim}}$  can be applied to analyze the size of a template fitted to interferometric visibilities or to image brightness distribution. Comparison of  $d_{\text{lim}}$  with the size obtained from the fit by a template can be used to separate valid measurements from upper limits.

Elliptical or circular Gaussian components are applied routinely for estimating sizes of emitting regions. The PSF is often also represented by an elliptical Gaussian shape. In the most general case an elliptical Gaussian component is described by its axes  $\theta_{\text{maj}}$ ,  $\theta_{\text{min}}$  and the position angle of the major axis  $\psi$ . Correspondingly, an elliptical PSF is given by  $(b_{\text{maj}}, b_{\text{min}}, \psi)$ . In this case, the resolution limit should be calculated for  $\theta_{\text{maj}}$  and  $\theta_{\text{min}}$ . The FWHM of the PSF is represented by its width  $b_{\psi}$  measured along the direction of the axis for which the limit is calculated. The corresponding resolution limit is then obtained from Eq. (40)

$$\theta_{\text{lim},\psi} = 2^{2-\beta/2} b_{\psi} \left[ \frac{\ln 2}{\pi} \ln \left( \frac{\text{SNR}}{\text{SNR} - 1} \right) \right]^{1/2}. \quad (51)$$

Whenever either of the two axes is smaller than its respective  $\theta_{\text{lim},\psi}$ , the size obtained from the fit by a Gaussian component should be treated as upper limit on the size of the emitting region.

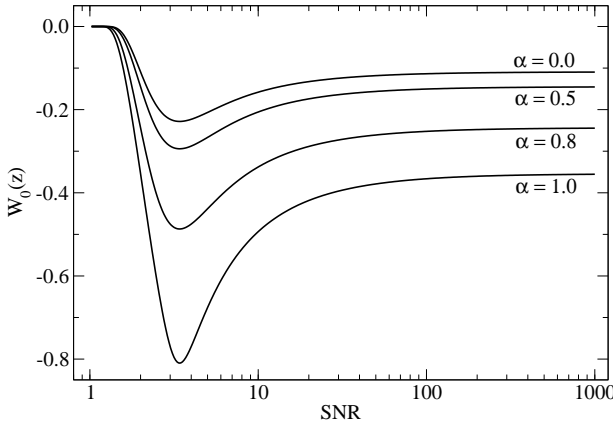


**Fig. 6.** Zero order product logarithm function  $W_0(\zeta)$  calculated for a range of shell width parameter  $\alpha$ .

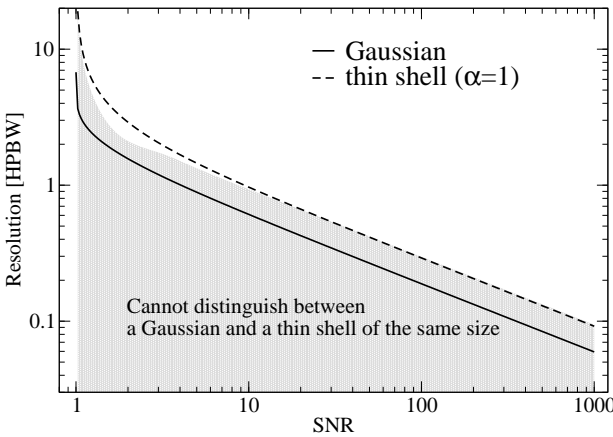


**Fig. 7.** Comparison of the resolution limits for a Gaussian and an infinitely thin spherical shell. The shaded area marks angular sizes for which a fit by a thin shell cannot be distinguished from a fit by a Gaussian of the same size.

## 6.2. Fine structure of young supernovae

In VLBI observations of early stages of supernova expansion, it is important to decide at which moment the observed brightness distribution can be identified with a shell-like structure, thus distinguishing it from another shape (for instance, a Gaussian or a uniform disk). Let us assume that the brightness distribution of emission from a young supernova is fit by a spherical shell of size  $d_s$  and thickness  $\alpha$ . The resolution criteria can then be used to establish whether (1) the fit is different from a fit by another template of the same size and (2) the fit can be distinguished from a fit by another template of arbitrary size. These two cases form the necessary and sufficient conditions for verifying the shell-like shape of the expanding remnant. A method for distinguishing between a shell and a Gaussian templates is described below. The same procedure can be used to derive criteria for distinguishing between any other pair of TBD.

To distinguish between a shell and a Gaussian component of the same size,  $d_{g,s}$ , the condition

$$f(V_s, V_g) = |\max(V_s - V_g)|_0^{q_{\max}} = \sigma_n = 1/SNR \quad (52)$$

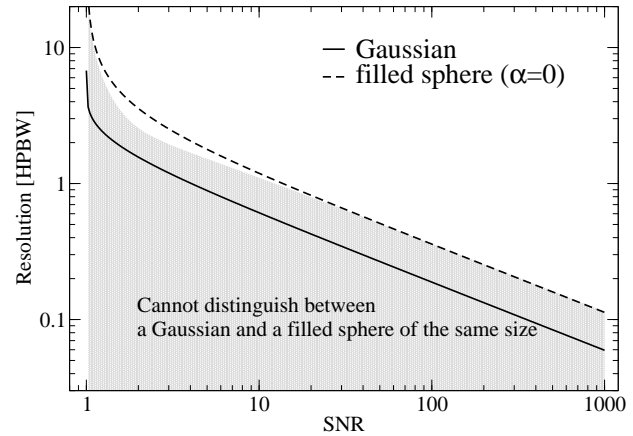


**Fig. 8.** Comparison of the resolution limits for a Gaussian and a filled sphere. The shaded area marks angular sizes for which a fit by a filled sphere cannot be distinguished from a fit by a Gaussian of the same size.

must be satisfied, where both the Gaussian ( $V_g$ ) and shell ( $V_s$ ) visibility amplitudes are normalized to unity at  $q = 0$ , as given by Eqs. (23) and (27). This condition applies only to  $d_{g,s}$  comparable or smaller than the HPBW. Setting  $HPBW \equiv 1$ , the visibility difference in Eq. (52) is maximized at  $q_{g,s} = 1/\sqrt{4\pi}$ . Equation (52) can then be rewritten as

$$\exp\left(\frac{1}{\lambda_1}\delta_d^2\right) + \frac{1}{\lambda_2}\delta_d^2 = \frac{1}{1-\sigma} = \frac{(SNR-1)^2+1}{SNR(SNR-1)}, \quad (53)$$

where  $\delta_d = \sqrt{d_{g,s}^2/(ab)}$  is the relative size of a template measured in units of HPBW, and  $\lambda_{1,2}$  are given by:

$$\lambda_1 = \frac{16 \ln 2}{\pi}, \quad \lambda_2 = \frac{40}{\pi} \left( \frac{1-\alpha^3}{1-\alpha^5} \right).$$

Denote

$$\xi_{SNR} = \frac{(SNR-1)^2+1}{SNR(SNR-1)}.$$

Solving Eq. (53) for  $\delta_d$  and recovering the angular size  $\sqrt{\delta_d^2 a b}$  yields the minimum size at which it is possible to distinguish between the spherical and Gaussian shapes

$$d_{lim,gs} = \sqrt{\frac{ab}{SNR}} [\lambda_2 \xi_{SNR} + \lambda_1 W_0(\zeta)]^{1/2}, \quad (54)$$

where

$$\zeta = -\frac{\lambda_2}{\lambda_1} \exp\left[-\frac{\lambda_2}{\lambda_1} \xi_{SNR}\right]$$

and  $W_0$  is the zero order product logarithm function described in Appendix B. Figure 6 shows the dependence of  $W_0(\zeta)$  on SNR and the shell width  $\alpha$ . The relevant range of  $SNR = [1, \infty]$  determines the range of  $\zeta$  ( $-1/e, 0$ ). Within this range, an approximation

$$W_0(\zeta) + (1 + \frac{1}{e})(\zeta + \frac{1}{e})^{1/e} - 1$$

can be used. The resulting limits on resolution are shown in Figs. 7–8 for a thin shell and filled sphere, respectively. In each

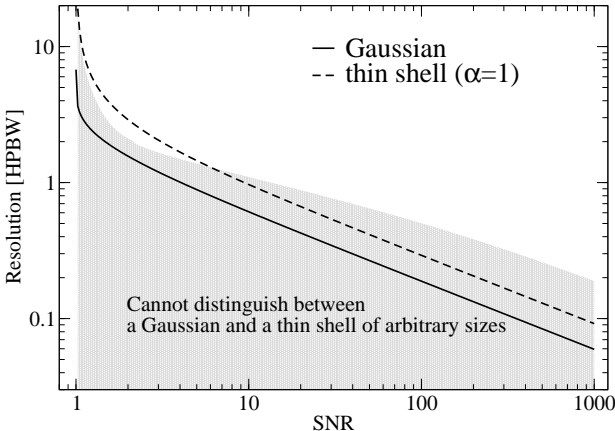


**Fig. 9.** Comparison of the resolution limits for a Gaussian and an infinitely thin spherical shell. The shaded area marks angular sizes for which a fit by a thin shell cannot be distinguished from a fit by a Gaussian of arbitrary size.

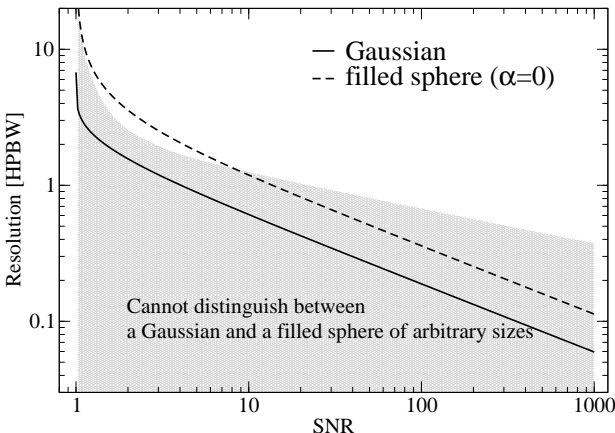


**Fig. 10.** Comparison of the resolution limits for a Gaussian and a filled sphere. The shaded area marks angular sizes for which a fit by a filled sphere cannot be distinguished from a fit by a Gaussian of arbitrary size.

figure, the shaded area indicate sizes for which it is not possible to distinguish between a Gaussian and a spherical shape of the same size. At large SNR levels this limit approaches the resolution limit for a spherical shape.

For a Gaussian and a shell of arbitrary sizes  $d_g$ ,  $d_s$ , the visibility difference reaches a maximum at  $q_{gs} \leq q_{\max}$ , which is determined by solving the equation  $df^2(V_g, V_s)/dq = 0$ . For each given  $d_s$  (or  $d_g$ , reciprocally), the minimum SNR at which one template can be distinguished from another is given by  $2/f(V_s, V_g)$  evaluated at  $q_{gs}$ . Below this SNR, it is not possible to claim that the template fit is unique. Application of this method is exemplified in Figs. 9–10 for a thin shell and filled sphere matched against a Gaussian. Similar approach can be applied to any other pair of templates.

## Appendix A: Resolution limits for selected templates

This appendix summarizes analytical expressions derived for the resolution factors  $\mathcal{R}_{\lim}$  and  $\mathcal{R}_{\text{res}}$  and limiting sizes  $d_{\lim}$  and  $d_{\text{res}}$ . The analytical expressions for  $\mathcal{R}_{\text{res}}$  and  $d_{\text{res}}$  are accurate within 40%. Empirical correction factors  $\kappa(SNR)$  are introduced to correct this inaccuracy. The correction reduces the errors to within 0.01% for  $\text{SNR} \leq 1000$ . At larger SNR, the correction factors become essentially constant.

### A.1. Spherical shell of finite thickness

$$d_{\lim} = \frac{2}{\pi} \left[ \frac{1 - \alpha^3}{1 - \alpha^5} \frac{5}{2(SNR - 1)} \right]^{1/2} S_q \mathcal{B}_c, \quad (\text{A.1})$$

$$\mathcal{R}_{\lim} = \frac{2}{\pi} \left[ \frac{1 - \alpha^3}{1 - \alpha^5} \frac{5}{2(SNR - 1)} \right]^{1/2}. \quad (\text{A.2})$$

For a rectangular, power-law SF and uniform weighting, the corresponding limiting resolution for a spherical shell becomes

$$d_{\lim} = \sqrt{\frac{40}{\pi} \left( \frac{1 - \alpha^3}{1 - \alpha^5} \right) \frac{ab}{SNR - 1}}. \quad (\text{A.3})$$

The two limiting cases of the spherical shell are described by the filled sphere ( $\alpha = 0$ ) and infinitely thin shell ( $\alpha \rightarrow 1$ ), which gives

$$d_{\lim, \text{sphere}} = \sqrt{\frac{40}{\pi} \frac{ab}{SNR - 1}}, \quad (\text{A.4})$$

$$d_{\lim, \text{shell}} = \sqrt{\frac{24}{\pi} \frac{ab}{SNR - 1}}. \quad (\text{A.5})$$

The largest detectable size is given by

$$d_{\text{res}} = \frac{2}{\pi} \Phi(SNR) \left[ \frac{5}{2} \frac{1 - \alpha^3}{1 - \alpha^5} \right]^{1/2} S_q \mathcal{B}_c, \quad (\text{A.6})$$

$$\mathcal{R}_{\text{res}} = \frac{2}{\pi} \Phi(SNR) \left[ \frac{5}{2} \frac{1 - \alpha^3}{1 - \alpha^5} \right]^{1/2}, \quad (\text{A.7})$$

where

$$\Phi(SNR) = SNR^{1/(3-\beta)} \left( \frac{SNR - 1}{SNR} \right)^{1/2}.$$

### A.2. Disk of uniform brightness

The resolution limit is given by

$$d_{\lim} = \frac{2}{\pi} \left[ \frac{2}{SNR - 1} \right]^{1/2} S_q \mathcal{B}_c, \quad (\text{A.8})$$

$$\mathcal{R}_{\lim} = \frac{2}{\pi} \left[ \frac{2}{SNR - 1} \right]^{1/2}. \quad (\text{A.9})$$

The largest detectable size is determined by

$$d_{\text{res}} = \frac{2}{\pi} \sqrt{2} \Phi(SNR) S_q \mathcal{B}_c, \quad (\text{A.10})$$

$$\mathcal{R}_{\text{res}} = \frac{2}{\pi} \sqrt{2} \Phi(SNR). \quad (\text{A.11})$$

### A.3. Ring

The resolution limit is given by

$$d_{\text{lim}} = \frac{2}{\pi} \left[ \frac{1}{SNR - 1} \right]^{1/2} S_q B_c, \quad (\text{A.12})$$

$$\mathcal{R}_{\text{lim}} = \frac{2}{\pi} \left[ \frac{1}{SNR - 1} \right]^{1/2}. \quad (\text{A.13})$$

The largest detectable size is described by

$$d_{\text{res}} = \frac{2}{\pi} \Phi(SNR) S_q B_c, \quad (\text{A.14})$$

$$\mathcal{R}_{\text{res}} = \frac{2}{\pi} \Phi(SNR). \quad (\text{A.15})$$

### A.4. Empirical corrections for $d_{\text{res}}$ and $\mathcal{R}_{\text{res}}$

Analytical expressions for  $d_{\text{res}}$  and  $\mathcal{R}_{\text{res}}$  must be corrected for the error of the Taylor expansion in the large-size limit. Thus, for the shell, disk, and ring templates

$$\mathcal{R}_{\text{res,corr}} = \kappa(SNR) \mathcal{R}_{\text{res}}, \quad (\text{A.16})$$

with the empirical correction factors  $\kappa(SNR)$  given by

$$\kappa(SNR) = 1 + a_1 \lg(a_2 \lg(SNR) + 1) + a_3 \lg\left(\frac{1}{a_4[\lg(SNR)]^2 + 1}\right). \quad (\text{A.17})$$

The coefficients  $a_1$ – $a_4$  are listed in Table A.1. At  $SNR \geq 300$ ,  $\kappa(SNR) \approx \text{const}$ , for all templates. The limiting values of  $\kappa(SNR)$  are given in Table A.1.

**Table A.1.** Coefficients for  $\kappa(SNR)$

	Sphere	Shell	Disk	Ring
$a_1$	8.95923	6.30926	6.87495	3.24248
$a_2$	0.11622	0.13358	0.13955	0.20988
$a_3$	2.23652	1.34282	1.69345	0.82607
$a_4$	0.12907	0.22302	0.17399	0.31843
$\kappa(SNR > 300)$	1.42	1.28	1.35	1.20

## Appendix B: Product logarithm function

The zero order product logarithm function  $W_0$  (Fig. B.1) provides the principal solution for  $w$  in the equation  $w \exp(w) = z(w)$ .  $W_0$  is the principal value of the Lambert  $W$ -function (Corless et al. 1996), and it is essentially an extension of the logarithm function.  $W_0$  is real-valued for  $z > -1/e$ .

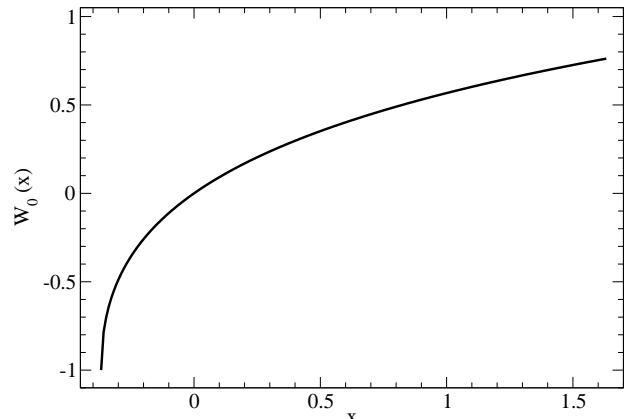


**Fig. B.1.** Zero order product logarithm function  $W_0$  plotted for a range of arguments that cover the small and the large argument asymptotics.

## References

Bartel, N., Bietenholz, M. F. 2003, ApJ, 591, 301  
 Bertero, M., De Mol, C. 1996, in *Progress in Optics*, ed. E. Wolf (Elsevier: Amsterdam), v. XXXVI, 129  
 Corless, R. M., Gonnet, G. H., Hare, D. E. G., Jeffrey, D. J., Knuth, D. E. 1996, *Adv. Comput. Math.* 5, 329  
 Briggs, D. S. 1995, PhD Dissertation, NMIMT, Socorro NM, USA  
 Briggs, D. S., Schwab, F. R., Sramek, R. A. 1999, in *ASP Conf. Ser.*, v. 180, *Synthesis imaging in radio astronomy II*, eds. Taylor, G. B., Carilli, C. L., Perley, R. A. (ASP: San Francisco), 127  
 Fomalont, E. B. 1999, in *ASP Conf. Ser.*, v. 180, *Synthesis imaging in radio astronomy II*, eds. Taylor, G. B., Carilli, C. L., Perley, R. A. (ASP: San Francisco), 301  
 Forward, R. L. 1978, *Phys. Rev. D*, 17, 379  
 Frieden, B. R. 1971, in *Progress in Optics*, ed. E. Wolf (Elsevier: Amsterdam), v. IX, 311  
 Hariharan, R., Sanders, B. C. 1996, in *Progress in Optics*, ed. E. Wolf (Elsevier: Amsterdam), v. XXXVI, 49  
 Horiuchi, S., Fomalont, E. B., Taylor, W. K., et al. 2004, ApJ, 616, 110  
 Kellermann, K. I. 2002, PASA, 19, 77  
 Kellermann, K. I., Paulini-Toth, I. I. K. 1969, ApJ, 155, L71  
 Kolobov, M. I., Fabre, C. 2000, *Phys. Rev. Lett.*, 85, 18, 3789  
 Lobanov, A. P. 2003, SKA Memo No. 38  
 Lobanov, A. P., Krichbaum, T. P., Graham, D. A., et al. 2000, *A&A*, 364, 391  
 Marcaide, J. M., Alberdi, A., Ros, E., et al. 1995, *Science*, 270, 1475  
 McDonald, A. R., Muxlow, T. W. B., Pedlar, A., et al. 2001, *MNRAS*, 322, 100  
 Moellenbrock, G. A., Fujisawa, K., Preston, R. A., et al. 1996, *AJ*, 111, 2174  
 Norton, R. H., Beer, R. 1976, *J. Opt. Soc. Amer.* 66, 259  
 Pearson, T. J. 1999, in *ASP Conf. Ser.*, v. 180, *Synthesis imaging in radio astronomy II*, eds. Taylor, G. B., Carilli, C. L., Perley, R. A. (ASP: San Francisco), 335  
 Pérez-Torres, M. A., Alberdi, A., Marcaide, J. M., et al. 2002, *MNRAS*, 335, L23  
 Rayleigh, J. W. S. 1879, *Phil. Mag.*, 8, 261  
 Stoughton, C., Lupton, R. H., Bernardi, M., et al. 2002, *AJ*, 123, 485  
 Tango, W. J., Davis, J. 2002, *MNRAS*, 333, 642  
 Taylor, G. B., Carilli, C. L., Perley, R. A. (eds.), *Synthesis imaging in radio astronomy II*, *ASP Conf. Ser.*, v. 180 (ASP: San Francisco)

Thompson, A. R., Moran, J. M., Swensson, G. W. 1986,  
Interferometry and Synthesis in Radio Astronomy, New York:  
Wiley.

Toraldo di Francia, G. 1969, J. Opt. Soc. Am., 59, 799